Proceedings of the ASME 2023 42nd International Conference on Ocean, Offshore and Arctic Engineering
OMAE2023
June 11-16, 2023, Melbourne, Australia

OMAE2023-101930

GRADIENT-BASED DESIGN OPTIMIZATION OF FULLY-FLEXIBLE FLOATING WIND TURBINES USING MODAL ANALYSIS

Peter J. Rohrer[1,*], Erin E. Bachynski-Polić[1], John Marius Hegseth[2],

[1]Norwegian University of Science and Technology, Trondheim, Norway
[2]Dr.Techn. Olav Olsen, Lysaker, Norway

ABSTRACT

A variety of substructure concepts for floating offshore wind have been developed. Design optimization can be used to efficiently explore this design space and guide further work. Previous design optimization studies have been limited by model simplifications, including the assumption of rigid body motions, lack of substructure flexibility, and a focus on a single floating foundation concept. High computational costs of gradient-free optimization methods have limited the number of design variables considered. In this work, gradient-based optimization methods and a frequency-domain modal analysis model based on three-dimensional modeshapes make it possible to consider a more detailed structural model with reasonable computational cost. This work implements a linearized aero-hydro-servo-elastic model of a tension-leg platform wind turbine. The optimization varies sizing parameters and the model computes responses to wind and wave forcing in multiple environmental conditions. The model computes forcing and response in generic modes rather than assuming rigid body motions. Implementation of the model with analytical gradients in OpenMDAO allows for efficient optimization with dozens of design variables. The optimization results show reduction of the objective while satisfying constraints. Furthermore, there is potential for this approach to be adapted to other floating wind turbine substructure designs.

Keywords: design optimization, floating wind turbine, tension-leg platform, OpenMDAO

1. INTRODUCTION

To meet growing demand and support increasingly large wind turbine designs, a variety of floating foundation concepts for offshore wind have been developed. Nonetheless there is still limited real-world experience with these concepts, and much of the design space remains unexplored. Multidisciplinary design optimization can efficiently explore the design space and inform further design work. Previous floating wind turbine design optimization studies have been limited by model simplifications or the use of gradient-free optimization approaches. Typical model simplifications have included the assumption of rigid body motions, the use of a small number of design variables, and a focus on a single floating foundation concept. These limitations have made it difficult to consider large flexible structures and detailed geometries. The high computational costs of gradient-free optimization algorithms have made it impractical to include constraints based on fatigue and extreme responses, or a sufficient number of design variables to account for structural design.

Structural flexibility (or elasticity) is often a concern for efficiently-designed large structures. Although structural deformations may be small, elasticity often leads to larger local stresses as well as the potential for resonant flexible responses. For large floating structures, the interaction of structural deformations and hydrodynamic loading, hydroelasticity, may be of interest. Borg et al. [1] found that including substructure flexibility was important for understanding sectional loads on a spar-buoy floating wind turbine, despite limited impact on global motions. Pegalajar-Jurado et al. [2] studied a 'semi-flexible' semi-submersible design which included a rigid body below the still waterline and flexible tower beginning at the still waterline, and found coupled bending frequencies were similar but not identical to a fully-flexible model. In the definition of a 10MW reference semi-submersible floating wind turbine, Müller et al. [3] found that the inclusion of substructure flexibility caused a 25% decrease in the first tower bending frequency. Silva de Souza and Bachynski [4] considered the effect of flexible pontoons for a tension-leg platform wind turbine substructure, and found considering pontoon flexibility was important for accurately predicting tower bending natural frequencies. However, hydroelastic effects were negligible: the deformations had limited effects on the hydrodynamic loading. State-of-the-art methods for time-domain coupled analysis floating wind turbines now often allow for the consideration of substructure flexibility in relatively complex structures, such as in

*Corresponding author: peter.j.rohrer@ntnu.no

recent work by Thomsen et al. [5] analyzing the TetraSpar concept. A broad review of offshore wind optimization by Chen and Kim [6] found previous optimizations often include tower or monopile flexibility, but few works had considered flexible floating substructures.

A number of specific challenges related to offshore wind turbine optimization are well outlined by Muskulus [7]. Some challenges of interest for floating wind are: the large number of environmental load cases that must be considered, and the significance of fatigue loads due to higher-order modes and local phenomena. An early attempt at design optimization of floating wind turbines by Fylling and Berthelsen [8] applied gradient-based optimization to a rigid spar-type floating wind turbine model with moorings and power cables. Their model included up to six design variables to describe the substructure for a 5 MW turbine. Their optimization was able to improve upon an unacceptable initial design, but had difficulties with inaccuracies in the approximated (finite difference) gradients.

Leimeister et al. [9] developed a framework for wind turbine optimization based on a generic coupled time-domain model and performed gradient-free multiobjective optimization of the OC3 spar-buoy floating wind turbine with only three design variables describing the substructure. Their objectives minimized platform motions and restricted accelerations and inclination based on a pre-selected design load condition that was deemed to be the critical condition. Other gradient-free optimization studies by Hall et al. [10] and Karimi et al. [11] considered a wider range of floating wind turbine concepts, however optimizations were generally limited to approximately ten design variables and rigid structures due to the computational cost of evaluating so many designs. Hegseth [12] developed a gradient-based design optimization model of a spar-type floating wind turbine with over 80 design variables using analytical gradients. Constraints on manufacturability, extreme response, and fatigue damage using up to 30 fatigue environmental conditions were applied with the objective of minimizing cost of the floating wind turbine and variation in power output. Hegseth's model considered combined substructure and tower flexibility, but only included a single two-dimensional bending mode and two rigid modes of response. Furthermore, the hydrodynamic formulation developed was only applicable to vertical cylinders.

This work builds on previous gradient-based optimization models for floating wind turbines; and introduces methods that can be applied to other large, flexible floating wind turbine structures. Gradient-based optimization methods using analytical derivatives and modal analysis make it possible to efficiently consider relatively detailed global structural models and multiple environmental conditions with reasonable computational cost. The analysis model developed consists of a finite element model and eigenvalue analysis specific to tension-leg platforms, while the methods for computing response based on three-dimensional mode shapes can be broadly applied to other flexible floating wind turbine designs.

2. MODEL DEVELOPMENT

The gradient-based optimization presented in this paper centers around a design model, TLPOpt. TLPOpt is a linearized aero-hydro-servo-elastic model of a flexible tension-leg platform floating wind turbine. The model can be roughly divided into two sections: a finite element model based on beam elements that interprets inputs and computes the coupled modeshapes of the floating wind turbine; and computation of responses in the frequency-domain based on modal analysis. Figure 1 shows the excitation, mass, damping, and stiffness considered in TLPOpt, excluding mass and stiffness in the finite element model. Turbine thrust, moment, aerodynamic torque, generator torque, and aerodynamic damping act at the hub of the turbine, which has a mass and inertia. Hydrodynamic excitation and viscous damping act on the submerged hull. Hydrostatic stiffness is applied at the still waterline, and tendon stiffness is applied at each tendon attachment point. A schematic of the optimization model arrangement is shown in Fig. 2. While only two environmental conditions are shown in the figure, any number of conditions can be included simultaneously in the model. The model has been developed for optimization of tension-leg platform floating wind turbines, but is adaptable to other floating wind turbine substructures with modifications to the 'design' portion of the model. The wind turbine blades, hub, and nacelle are excluded from the optimization design space, and are modeled in a simplified manner. This allows the use of pre-calculated coefficients to determine aerodynamic forcing and damping. Additionally, while the model is capable of considering a large number of design variables describing structural design, it is not well-suited for prediction of complex local loading scenarios that would typically be considered in a detail-design stage. Additional details on the development of TLPOpt can be found in previous work by Rohrer et al. [13]

2.1 Equation of Motion

To enable efficient analysis and the use of gradient-based optimization methods, TLPOpt computes responses in the frequency-domain using transfer functions to relate responses of interest to excitation. The equations of motion are developed

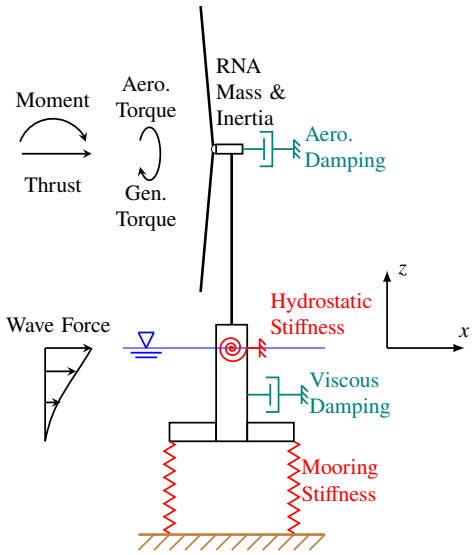

FIGURE 1: EXCITATION, MASS, DAMPING, AND STIFFNESS IN TLPOPT

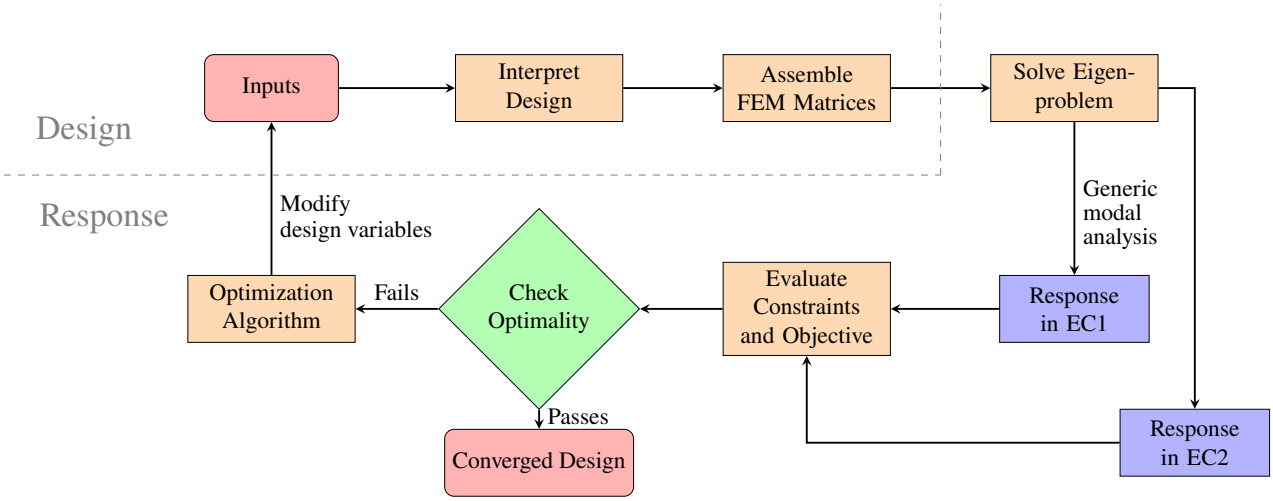

FIGURE 2: FLOWCHART OF OPTIMIZATION MODEL SHOWING DESIGN AND RESPONSE SECTIONS

in the state-space so that the structure and control systems are included simultaneously as a single closed loop system. To model the flexible structure of the floating wind turbine, TLPOpt uses modes of response from the eigenvalue analysis of the finite element model, described in Section 2.2. The total response is represented by the first ten (lowest natural frequency) modes in the present work. For many designs, the six rigid body modes appear within the first ten modes. Modal mass ($\mathbf{M_\Phi}$), stiffness ($\mathbf{K_\Phi}$), and structural damping matrices ($\mathbf{B_\Phi}$) are given in Eqs. (1) to (3), based on the modal equations and reduction of order in Cook [14], Chapter 11. The modal matrices are square matrices of size m where m is the number of modes used to represent the total response. The finite element model mass matrix ($\mathbf{M}$) and stiffness matrix ($\mathbf{K}$) are square matrices of size n, where n is the number of degrees of freedom in the model. The reduced basis eigenvector matrix $\mathbf{\Phi_m}$ is an n by m matrix. Mass normalization of eigenvectors (following Eq. (1)) leads to diagonal modal mass and stiffness matrices. By assuming modal damping and neglecting radiation damping (as discussed in Section 2.3) the damping matrix is also diagonal. The eigenvalue in each mode is ω_i^2, corresponding to a natural frequency of ω_i. The modal damping ratio applied in each mode is ζ_i.

$$\mathbf{M_\Phi} = \mathbf{\Phi_m}^T \mathbf{M} \mathbf{\Phi_m} = \lceil \mathbf{I} \rfloor \tag{1}$$

$$\mathbf{K_\Phi} = \mathbf{\Phi_m}^T \mathbf{K} \mathbf{\Phi_m} = \lceil \omega_i^2 \rfloor \tag{2}$$

$$\mathbf{B_\Phi} = 2\vec{\zeta} \cdot \sqrt{\mathbf{\Phi_m}^T \mathbf{K} \mathbf{\Phi_m}} = \lceil 2\zeta_i \omega_i \rfloor \tag{3}$$

Further details on the combination of the structural and controls model and the transfer function in the state-space are given in Appendix A.

2.2 Finite Element Model

TLPOpt represents the tension-leg platform structure with a three-dimensional finite element model. Figure 3 depicts the model with three dimensional cross-sections and nodal locations shown. A minimum of 40 elements are used for analysis, and the number of elements can be modified outside of the optimization loop. All elements in the tower, central column, and pontoons are represented by Euler-Bernoulli beam elements. The tower and column are represented by circular cross-section, hollow beam elements; while the pontoons are represented by square cross-section, hollow beam elements. Mass and stiffness (geometric and material) are defined in each element's local axes, and transformed to the global axes before assembly of the system matrices. Rigid links (shown in blue in Fig. 3) are utilized to connect the pontoon elements with the central column, and to attach the rotor-nacelle assembly. The use of these rigid links neglects local flexibility at these connections. Point masses are added to represent ballast in the central column (if needed) and the rotor-nacelle assembly. Point stiffnesses are applied to account for hydrostatic stiffness and the linear springs representing the tendons. The bending stiffness of the tendons is neglected, while the linear springs representing the tendons are a boundary condition enforced on the model. Modal damping equal to 1% of critical damping is applied to each mode to account for the uncertain structural damping.

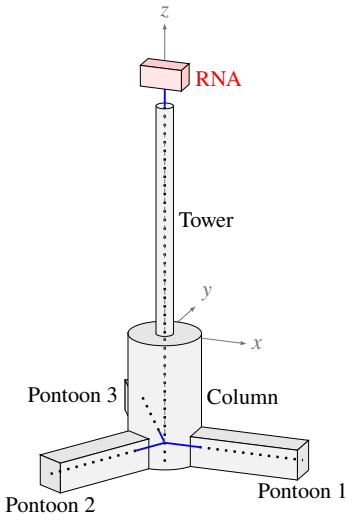

FIGURE 3: FINITE ELEMENT MODEL IN TLPOPT

2.3 Hydrodynamic Excitation and Damping

Hydrodynamic excitation is calculated using two linear wave load approximations, applied in modal (or generalized) coordinates following work by Newman [15]. Wave loading on the central column is calculated using MacCamy-Fuchs's theory [16], which is based on an analytic solution of the diffraction problem for a vertical circular cylinder. Wave loading on the pontoons is based on the MOJS (Morison's) equation [17], with both horizontal and vertical wave particle kinematics considered and accounting for the orientation of pontoons. A Froude-Krylov forcing term is included on the ends of all submerged members. Wave loading is calculated at specified wave frequencies, which are bounded to avoid very low frequencies and high frequencies where there is little wave excitation, to assemble a total hydrodynamic excitation transfer function. The modal excitation on the column and pontoons are combined in complex-space: relative phasing is preserved, but hydrodynamic interactions between the column and pontoons are neglected. Wave loading on the tendons is not considered, nor are mean wave loads or current-effects. Verification of the wave load approximation is discussed in Section 3.

Viscous damping is approximated for both the main column and pontoons using the widely-used Borgman form linearization of the drag term in the MOJS equation [18]. Constant 2D drag coefficients from DNV [19] are used. The linearization relies on the standard deviation of structural velocity, creating a cyclic dependence in the model that must be solved iteratively. Radiation damping is neglected, as resonant frequencies are typically far from frequencies where wave radiation is significant.

Added mass effects are considered for all submerged elements in three dimensions, using a strip theory approach and constant added mass coefficients from DNV [19]. Added mass is included in the mass finite element model mass matrix, leading to 'wet' natural modes for the structure. Normal added mass, tangential added mass, and axial added mass (end effects) are all included in the mass matrix, though normal added mass dominates.

2.4 Aerodynamic Excitation and Damping

TLPOpt makes use of a linearized quasi-steady version of blade element momentum theory (BEM), as is typical among aero-hydro-servo-elastic models. Two common corrections are applied to the BEM model used: the Prandtl correction for loss at the hub and tips, and the Glauert correction for high induction factors; considered by Burton [20] to be the minimum corrections needed. Both dynamic wake and dynamic stall effects are neglected, as well as aero-elasticity.

To accelerate computation, induction factors (to be used in the BEM calculation) can be computed and stored for wide ranges of blade pitch angles and tip-speed ratios. Only the final loads are needed to interface with the coupled model, so a rotor effective wind speed can be established to represent the rotor loads with a scalar value. A detailed derivation of this approach is summarized in Hegseth's PhD thesis [12].

2.5 Control System

Design of blade pitch and generator torque control systems is often considered a detailed design step and can be influenced by a number of site or operator specific factors. TLPOpt makes use of the well-known baseline blade-pitch controller from the NREL 5MW reference turbine [21] with a simplified low-pass filter and no transition strategy. The control system parameters (proportional and integral gains) are variables in the model and can be included as design variables. In the present work, the values for the land-based DTU 10MW reference turbine [22] are applied. The state-space equations of motion (detailed in Appendix A) allow for more implementation of advanced controls systems with more states, inputs, and outputs in future studies.

3. MODEL VERIFICATION

Verification of the responses of TLPOpt to irregular wave and turbulent wind excitation is presented in Fig. 4. For comparison a baseline tension-leg platform design from Tian's masters thesis [23] is modeled in SIMA, a nonlinear aero-hydro-servo-elastic analysis tool developed by SINTEF Ocean [24, 25]. The baseline design is a tension-leg platform substructure to support the DTU 10MW reference turbine [22]. The model in SIMA closely follows the modeling strategy of TLPOpt with a finite element model of beam elements representing the combined tower, column, and pontoons structure. Two notable differences between TLPOpt and SIMA are the modeling of the rotor and tendons. The SIMA model considers a spinning rotor and models the blades as beams, while TLPOpt models the entire RNA as a rigid body. Beam elements are used to represent the tendons in SIMA which provides more realistic modeling of tendon nonlinearities. Time-domain simulations with the same incoming wave spectrum are conducted in SIMA and post-processed to compare with frequency-domain response spectra and standard deviations from TLPOpt. Verification against another software tool introduces additional uncertainties, though verification with software is unavoidable given the lack of benchmark experimental results for tension-leg platform wind turbines.

The verification of bending moments shown in Fig. 4a suggests that TLPOpt is capable of capturing structural responses to wave-only excitation in the coupled model with reasonable accuracy. The response in both SIMA and TLPOpt is dominated by a wave-frequency component and a resonant peak at the tower bending frequency. The agreement between the magnitude of the bending moment is best in the transition from column to tower, and slightly less good at both the tower base and tower top. At the tower top the discrepancy is believed to be due to slight differences in the definition of the rotor-nacelle assembly inertia and the flexibility of blades in SIMA. Differences at the tower bending natural frequency (roughly 0.27 Hz) are due to coupling of the blade and tower bending in SIMA.

In Fig. 4b, tower bending moments are verified in a combined irregular wave and turbulent wind environment. While TLPOpt captures the shape of the response spectra well, SIMA results show a large increase in response magnitude in the wave frequency range which TLPOpt does not. This is believed to be due to interactions with the blade-pitch controller (which is not tuned for a tension-leg platform floating wind turbine) and wave-induced motions that are most apparent near the turbine's rated windspeed of $11.4\,\mathrm{m\,s^{-1}}$. Previous work (see Rohrer et al. [13] and Hegseth et al. [26]) found the simplified BEM model used

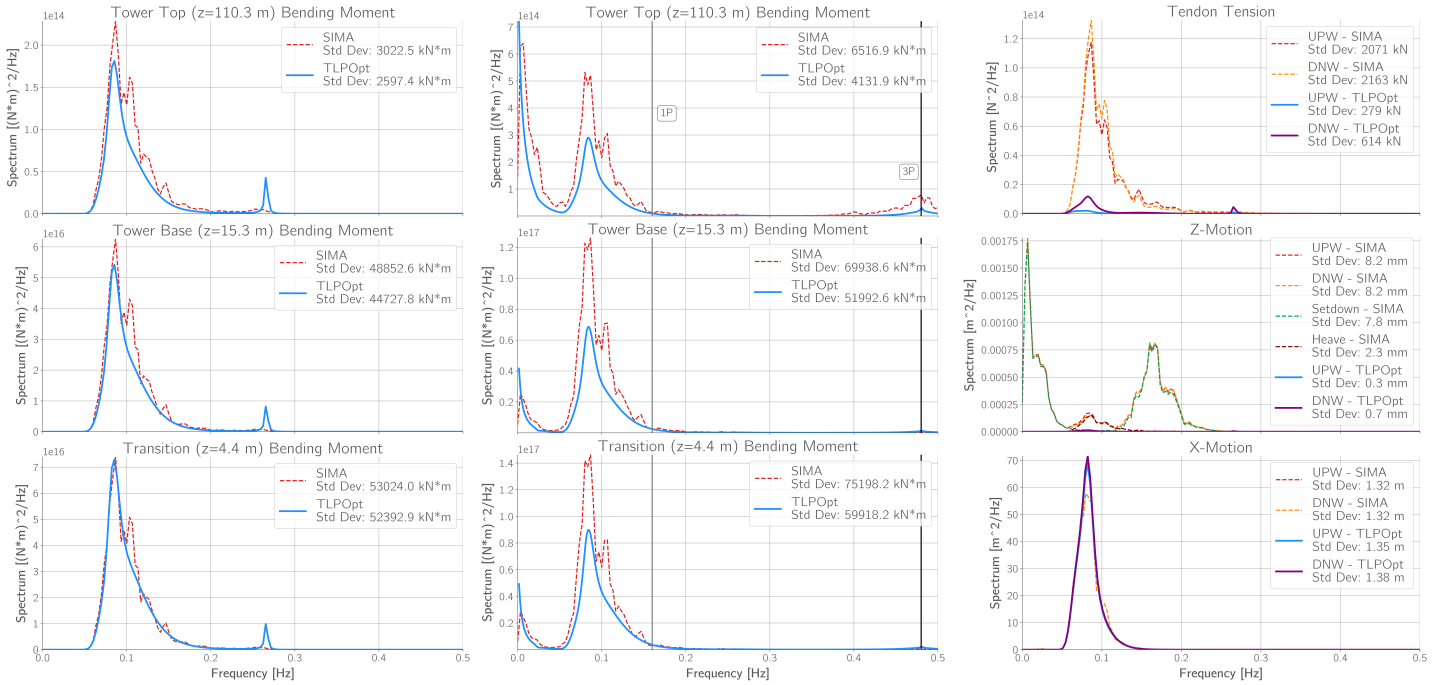

(a) Wave-only bending moment response JONSWAP spectrum: H_S = 7.5 m, T_p = 12 s

(b) Wave-Wind bending moment response JONSWAP spectrum: H_S = 7.5 m, T_p = 12 s Kaimal Turbulence U_0 = 11 m/s

(c) Wave-only tendon top response JONSWAP spectrum: H_S = 7.5 m, T_p = 12 s

FIGURE 4: WAVE AND WIND RESPONSE VERFICATION

in TLPOpt results in similar aerodynamic load spectra as dynamic BEM results from nonlinear aero-hydro-servo-elastic time domain analysis.

A verification of tendon top tensions and displacements shown in Fig. 4c suggests that TLPOpt is capable of capturing wave-induced horizontal displacements, but struggles to fully capture tendon top vertical motions and tendon tensions. Horizontal motions are dominated by wave-frequency response, and TLPOpt predicts the standard deviation of horizontal response within 5% of SIMA results. Tendon tension results show that TLPOpt captures a small wave-frequency tension response and an exaggerated difference between upwave and downwave tendons, but significantly underpredicts the standard deviation of tendon tensions. The vertical motion responses show that TLPOpt also fails to capture a significant portion of the wave-frequency vertical motion, as well as low-frequency and high-frequency vertical motion responses. The bulk of this underprediction is due to not modeling set-down, the nonlinear heave motion that is coupled with surge/sway motions in tension-leg platforms. Figure 4c also includes spectra for an approximation of set-down vertical motion and pure heave vertical motion based on the SIMA time-domain results. These show that the majority of vertical motion seen in SIMA results can explained by set-down. Set-down has been neglected thus far in the model as it is specific to tension-leg platforms and design of tendons is not a specific goal of this model. Several options to include a set-down effect exist, including statistical linearization proposed by Low [27] or modeling the tendons in the finite element model.

A comparison of the hydrodynamic transfer functions between TLPOpt and WAMIT for the second, fifth, seventh, and eighth mode are shown in Fig. 5. WAMIT [28] is a commercially available software for wave-structure interaction based on potential theory that can consider wave loading in generalized modes of deformation. For the baseline design, the second mode is roughly equivalent to the rigid body surge mode, the fifth mode is the first combined bending mode in the XZ-plane, the seventh mode is similar to the rigid body heave mode, and the eighth mode is the second combined bending mode in the XZ-plane. The results show qualitative agreement between the hydrodynamic transfer functions from the approximations and WAMIT results, with the best agreement seen in mode two and mode five, the lowest frequency modes shown. Mode seven is similar to the rigid body heave mode, though flexible pontoons mean the heave displacement, and therefore excitation, is not equivalent as seen in the comparison of WAMIT results for rigid heave and mode seven. Excitation is undepredicted by TLPOpt for both mode seven and mode eight, possibly due to the inability to consider interaction between the column and pontoons in the TLPOpt model.

4. OPTIMIZATION PROBLEM

The TLPOpt model described above is used to conduct gradient-based design optimization by posing a formal optimization problem. The optimization problem consists of design variables that the optimizer can vary, constraint functions to limit the feasible design space, and an objective function that the optimization intends to minimize. Therefore the optimization problem can be rewritten as a set of coupled equations. The problem can be said to be 'multidisciplinary' because the design variables, con-

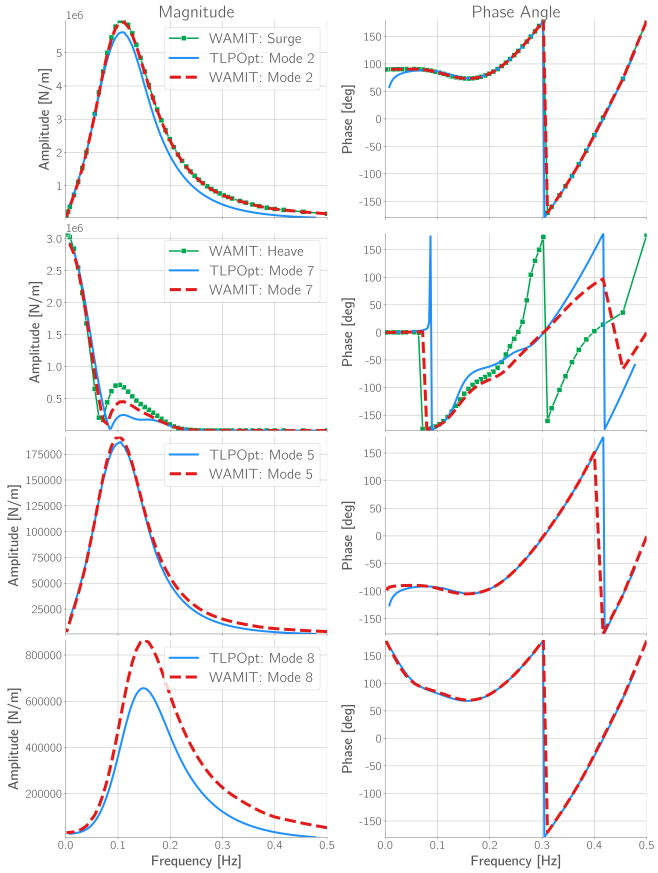

FIGURE 5: HYDRODYNAMIC TRANSFER FUNCTION VERIFICATION IN SELECTED MODES.

straints, and objective span several analysis disciplines. A formal definition of this problem can be found in Chapter 1 of Martins and Ning [29]. The optimization problem is assembled in the OpenMDAO framework [30], an open-source tool for developing multidisciplinary optimization models with a focus on gradient-based optimization. OpenMDAO acts as an interface between the model representing the physical response of the floating wind turbine and the mathematical model that the optimization algorithm solves. OpenMDAO implements PyOptSparse [31, 32], which provides Python implementations of several optimization algorithms and exploits sparsity in the coupled equations that form the optimization problem. Specifically, the combination of OpenMDAO and PyOptSparse allows for efficient computation of coupled derivatives for large problems (i.e. gradients of the objective with respect to the design variables) using the *modular analysis and unified derivatives* (MAUD) architecture developed by Hwang and Martins [32]. The SNOPT [33] optimization algorithm was used based on previous work by Hegseth [12]. SNOPT implements a sequential quadratic programming algorithm, and is effective at optimization of problems with computationally expensive objective or constraint functions. The implementation of TLPOpt in OpenMDAO makes it possible to quickly formulate a wide variety of optimization problems, such as the specific problem considered in this work is described below.

4.1 Problem formulation

The problem formulation presented here demonstrates the potential for gradient-based design optimization of flexible floating wind turbines, but is not a unique formulation. An infinite number of combinations of design variables, constraints, and objectives can be developed based on the goals of the optimization. Each problem formulation developed requires attention to scaling of the model to ensure optimization convergence. TLPOpt is defined in physical units, with inputs and outputs spanning many orders of magnitude (ex: thicknesses in mm and stresses in MPa), meaning scaling is crucial for reasonable consideration of all design variables, objectives and constraints. All optimizations were run on a workstation PC using a single processor core in under one hour, however the implementation of some components requires large amounts (~100 GB) of memory to calculate analytical gradients.

4.1.1 Design Variables. The design variables describe the geometry of the tension-leg platform substructure, and are listed in Table 1. A total of 28 design variables are considered in the current model. The finite element model considers vectorized inputs describing the diameter and thickness of the tower and column, side length and thickness of the pontoons, and scalar inputs for column draft, pontoon length, tendon diameter, and ballast factor. To reduce the number of design variables, vectorized inputs are described by shorter vectors of four spline control points. These control points are fitted with B-splines in OpenMDAO using an approach from Hwang and Martins [34]. Additional design variables describe the platform draft, pontoon length, outer diameter of the tendons, and amount of ballast weight added to the design. The bounds for each design variable, which strictly limit the values the optimization algorithm will explore, are given in Appendix B.

TABLE 1: DESIGN VARIABLES IMPLEMENTED IN TLPOPT

Variable	Units	Meaning
D_{tower}	[m]	Outer diameters of tower segments.
t_{tower}	[mm]	Wall thicknesses of tower segments.
D_{column}	[m]	Outer diameters of main column segments.
t_{column}	[mm]	Wall thicknesses of main column segments.
T	[m]	Draft of main column.
$s_{pontoon}$	[m]	Outer side-lengths of pontoon segments.
$t_{pontoon}$	[mm]	Wall thicknesses of pontoon segments.
L_p	[m]	Length of pontoons. (column to pontoon tip)
D_{tend}	[m]	Outer diameter of tendons.
BF	[-]	Ballast weight as a fraction of column displacement.

4.1.2 Constraints. Constraints limit the feasible design space for optimization. A particular challenge is definition of a set of constraints that are sufficient to develop a realistic design but not overly limiting. Many optimization algorithms (including SNOPT) must evaluate functions and gradients outside the feasible region, so constraint functions must return a reasonable value even when violated. This leads to creative redefinition of certain constraints or components to ensure a logical return. The bounds chosen for the design variables are not formally constraints, as

the optimizer has no ability to consider values outside design variable bounds.

The first set of constraints introduced is design constraints, referred to as 'static' because they consider a calm-water, no-wind case. These represent constraints that might be applied to ensure manufacturability, or allow for unimpeded maintenance access. A constraint is applied to column, tower, and pontoon outer dimensions to limit the diameter taper angle to 10°. An additional constraint requires the diameter at the column top to be greater than or equal to that of the tower base. Finally, a constraint requiring positive pretension in all tendons (buoyancy greater than weight) is applied.

The second set of 'dynamic' constraints is applied to the response in three environmental conditions given in Table 2. The short-term extreme response in each of the three environmental conditions is checked simultaneously. A vectorized tower buckling constraint is applied using Eq. (4).

$$\sigma_x < \frac{\sigma_\sigma}{\gamma_M \gamma_F} \tag{4}$$

Where σ_x is axial stress at the tower outer radius, and σ_σ is the critical buckling stress found according to Eurocode 3 [35]. The material factor ($\gamma_M = 1.10$) and load factor ($\gamma_F = 1.35$) recommended by DNV GL are used [36, 37]. Surge displacement at the still water line is limited to 10% of water depth (20 m for this study) to avoid excessive tendon angles. A minimum dynamic tendon tension constraint (minimum of ten percent of pretension) is applied to the tendons to avoid slacking, and a constraint on maximum tendon stress at yield stress ($\sigma_Y = 355$ MPa) is applied for a simple model of maximum tendon tension. Short-term extreme responses in each environmental condition are calculated assuming the response variables are Gaussian processes using the average upcrossing rate (AUR) method [38], given in Eq. (5). In Eq. (5), $\xi(T)$ represents the most-probable maximum response, $\bar{x}$ is the mean response, σ_x is the standard deviation, $\nu_x^+(0)$ is the zero-upcrossing rate, and T is the short-term period length, in this case one hour. No additional safety factors are considered for the purposes of this study, though for practical purposes constraint limits could be adjusted to reflect safety factors.

$$\xi(T) = \bar{x} + \sigma_x \sqrt{2 \ln\left(\nu_x^+(0) T\right)} \tag{5}$$

4.1.3 Objective. The objective is a simple summation of steel mass, the mass of one tendon, and ten percent of ballast mass. The mass of a single tendon is used to avoid unfair 'preference' towards tendon mass in the optimization. Only ten percent of ballast mass is included to roughly reflect the difference in cost between ballast and steel mass. This serves as a simple approximation of the materials usage and cost of the design.

4.2 Analytical Gradients

To enable efficient gradient-based optimization, TLPOpt defines analytical gradients for the entire model. OpenMDAO allows users to define partial derivatives at the component level, often equivalent to a single function, and uses these defined partials to calculate total derivatives using the MAUD architecture. Gradient-based optimization algorithms perform best when provided smooth, continuous gradients (and some require continuity), so robust and correct definition of analytic partial derivatives is key to successful optimization.

5. OPTIMIZATION RESULTS

Results of the optimization are shown in Table 3 for the baseline design and the two different 'levels' of constraints applied to the model. The first level applies only the 'static' or design constraints described above. The second level imposes the same design constraints with additional 'dynamic' constraints on response in three environmental conditions, given in Table 2. These three environmental conditions are based on the 50-year contour surface of a joint probability distribution by Johannessen et al. [39] for the Northern North Sea. EC1 has a wind speed close to the turbine's rated wind speed, EC2 is near cut-out wind speed, and EC3 is above cut-out wind speed.

The baseline design used is modified from Tian's thesis [23] which described a tension-leg platform for the DTU 10MW reference turbine. The applied modifications are increased structural thicknesses and tower dimensions to have a feasible initial design. SNOPT does not require that the initial point in the optimization is feasible, though optimizer robustness and speed are improved by starting at a feasible point.

TABLE 2: ENVIRONMENTAL CONDITIONS CONSIDERED

Parameter	Units	EC1	EC2	EC3
Mean Wind Speed at Hub	[m s^{-1}]	11.0	21.0	50.0
Significant Wave Height	[m]	7.5	9.9	15.1
Spectral Peak Period	[s]	12.0	14.0	16.0

The results in Table 3 show designs that have converged with a relatively weak optimality tolerance, indicating the optimization makes progress in reducing the objective function while respecting the constraints.

The static case converges at the lower bound of all design variables. This leads to a dramatic decrease in the hull volume and objective mass, and the elimination of ballast mass. However, the design violates nearly all dynamic response constraints (which were not enforced in this optimization) with slacking tendons and tendon and tower stress in excess of yield stress.

The dynamic case shows a significant decrease in objective mass compared to the initial design, though less than in the static case. The converged design reduces tower and substructure mass, while increasing ballast mass. The substructure design follows expected patterns, with larger diameters at the base of the column, while minimizing diameter at the still waterline. The dynamic case does not appear to be on the edge of the feasible region in all response constraints, suggesting that the optimization may have exited prematurely or the design variable bounds may be too conservative. Figure 6 shows the tower dimensions and stress utilization (maximum stress as a fraction of maximum allowable given in Eq. (4)) along the length of the tower for the baseline and dynamic case. The dynamic case results in all tower wall thicknesses being at the lower bound and there is significant 'excess' stress capacity in the converged tower design. It is likely

that with the addition of tower fatigue constraints a more realistic thickness distribution is possible.

TABLE 3: SELECTED CONVERGED DESIGNS

Variable	Units	Baseline	Static	Dynamic
Tendon Diameter	[m]	2.70	0.50	1.52
Tendon Pretension	[kN]	20,781	9733	28,458
Hull Volume	[m^3]	17,226	5962	17,874
Volume in Pontoons	[%]	37.4	48.3	27.9
Tower Steel Mass	[t]	3427	1344	2260
Substruc. Steel Mass	[t]	2772	1113	2222
Ballast Mass	[t]	4423	0.0	4457
Column Draft	[m]	35.3	25.0	36.8
Center of Grav.	[m]	6.70	47.7	1.62
Center of Buoy.	[m]	-21.8	-15.1	-23.9
Max. Surge*	[m]	19.84	12.94	12.87
Min. Tend. Tension*	[kN]	9065	-122,907	16,752
Max. Tend. Stress*	[MPa]	43.5	5553	170
Max. Tow. Base Stress*	[MPa]	40.1	420	66.1
Objective Mass	[t]	7633	2493	5225

* most probable minimum/maximum in EC3

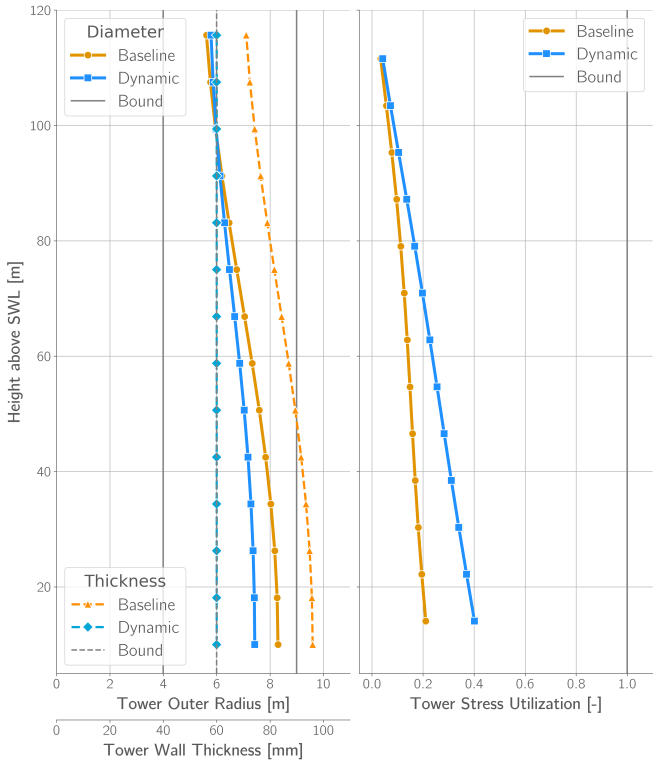

FIGURE 6: TOWER DIMENSIONS AND STRESS UTILIZATION FOR BASELINE AND CONVERGED DESIGN.

5.1 Model Limitations

The model and results presented in this work demonstrate the potential for gradient-based design optimization of floating wind turbines, but are subject to some key limitations which motivate future work towards practical gradient-based optimization. Discrepancies between responses from time-domain aero-hydro-servo-elastic codes and TLPOpt discussed above, especially concerning tendon tension variation, limit the ability of the model to consider extreme tension or tendon stress constraints. To better model structural design, stiffeners should be included in the model rather than assuming shell structures. Finally, constraints based on fatigue limit states should be considered to better reflect realistic loading scenarios and allow for appropriate structural sizing. Classification society rules can be implemented as constraints in the model to mirror current industry design practices.

In addition to development of the constraints, future work should focus on developing objective functions that better capture the design throughout its lifetime. The objective function applied in this work is deliberately simple, and does not include key portions of the cost including construction complexity, installation, maintenance, and decommissioning. An objective function could also seek to minimize environmental or community impact, while satisfying the same physical design constraints.

As with all optimization algorithms, SNOPT finds local minima. The algorithm is designed to seek global optimality, but it is impossible to definitively find global minima. Further work is needed to confirm the converged design represent optima, such as starting the optimization at several initial designs to ensure the same optima is found. More detailed views of trends in objective and constraint values, and variation of the initial point for optimization can both provide more information on the results.

6. CONCLUSION

This work has presented an improved version of the TLPOpt model, an optimization model for flexible tension-leg platform wind turbines, and initial optimization results demonstrating the potential for gradient-based optimization of floating wind turbines. The model shows reasonable agreement with time-domain analyses for global structural responses, and has been implemented in the OpenMDAO framework for multidisciplinary optimization. Results from optimizations show that the model is capable of considering stochastic response constraints in multiple environmental conditions simultaneously. Further model verification and refinement of optimization problem formulation are needed to produce more practical results. Finally the model is developed to consider generic designs, and can be quite easily adapted or extended to consider other floating wind turbine substructure designs.

ACKNOWLEDGMENTS

This work has been funded by the Research Council of Norway, through SFI BLUES, grant number 309281.

REFERENCES

[1] Borg, M., Hansen, A. M. and Bredmose, H. "Floating Substructure Flexibility of Large-volume 10MW Offshore Wind Turbine Platforms in Dynamic Calculations." *Journal of Physics: Conference Series* Vol. 753 (2016): p. 082024. DOI 10.1088/1742-6596/753/8/082024.

[2] Pegalajar-Jurado, A., Borg, M., Robertson, A., Jonkman, J. and Bredmose, H. "Effect of Second-Order and Fully Non-

linear Wave Kinematics on a Tension-Leg-Platform Wind Turbine in Extreme Wave Conditions." Trondheim, Norway, June 25-30, 2017, 2017. American Society of Mechanical Engineers. DOI 10.1115/OMAE2017-61798.

[3] Müller, K., Lemmer, F. and Yu, W. "LIFES50+ D4.2: Public Definition of the Two LIFES50+ 10MW Floater Concepts." Technical report. University of Stuttgart. 2018.

[4] de Souza, C. E. S. and Bachynski, E. E. "Effects of Hull Flexibility on the Structural Dynamics of a Tension Leg Platform Floating Wind Turbine." *Journal of Offshore Mechanics and Arctic Engineering* Vol. 142 No. 1 (2019). DOI 10.1115/1.4044725.

[5] Thomsen, J. B., Bergua, R., Jonkman, J., Robertson, A., Mendoza, N., Brown, C., Galinos, C. and Stiesdal, H. "Modeling the TetraSpar Floating Offshore Wind Turbine Foundation as a Flexible Structure in OrcaFlex and OpenFAST." *Energies* Vol. 14 No. 23 (2021): p. 7866. DOI 10.3390/en14237866.

[6] Chen, J. and Kim, M.-H. "Review of Recent Offshore Wind Turbine Research and Optimization Methodologies in Their Design." *Journal of Marine Science and Engineering* Vol. 10 No. 1 (2021): p. 28. DOI 10.3390/jmse10010028.

[7] Muskulus, M. and Schafhirt, S. "Design Optimization of Wind Turbine Support Structures—A Review." *Journal of Ocean and Wind Energy* Vol. 1 No. 1 : pp. 12–22.

[8] Fylling, I. and Berthelsen, P. A. "WINDOPT: An Optimization Tool for Floating Support Structures for Deep Water Wind Turbines." *ASME 2011 30th International Conference on Ocean, Offshore and Arctic Engineering*: pp. 767–776. 2011. DOI 10.1115/OMAE2011-49985.

[9] Leimeister, M., Kolios, A. and Collu, M. "Development of a Framework for Wind Turbine Design and Optimization." *Modelling* Vol. 2 No. 1 (2021): pp. 105–128. DOI 10.3390/modelling2010006.

[10] Hall, M., Buckham, B. and Crawford, C. "Evolving offshore wind: A genetic algorithm-based support structure optimization framework for floating wind turbines." *2013 MTS/IEEE OCEANS - Bergen*: pp. 1–10. 2013. DOI 10.1109/OCEANS-Bergen.2013.6608173.

[11] Karimi, M., Hall, M., Buckham, B. and Crawford, C. "A Multi-Objective Design Optimization Approach for Floating Offshore Wind Turbine Support Structures." *Journal of Ocean Engineering and Marine Energy* Vol. 3 No. 1 (2017): pp. 69–87. DOI 10.1007/s40722-016-0072-4.

[12] Hegseth, J. M. "Efficient Modelling and Design Optimization of Large Floating Wind Turbines." Ph.D. Thesis, Norwegian University of Science and Technology. 2020.

[13] Rohrer, P. J., Bachynski-Polić, E. E. and Collette, M. "Towards gradient-based design optimization of fully-flexible tension-leg platform wind turbines." *Journal of Physics: Conference Series* Vol. 2362 No. 1 (2022): p. 012033. DOI 10.1088/1742-6596/2362/1/012033.

[14] Cook, R. D., Malkus, D. S. and Plesha, M. E. *Concepts and Applications of Finite Element Analysis*, 3rd ed. Wiley.

[15] Newman, J. N. "Wave Effects on Deformable Bodies." *Applied Ocean Research* Vol. 16 No. 1 : pp. 47–59. DOI 10.1016/0141-1187(94)90013-2.

[16] MacCamy, R. and Fuchs, R. A. "Wave Forces on Piles: A Diffraction Theory." Technical Memorandum 69. Beach Erosion Board, Corps of Engineers. 1954.

[17] Morison, J., Johnson, J. and Schaaf, S. "The Force Exerted by Surface Waves on Piles." *Journal of Petroleum Technology* Vol. 2 No. 05 (1950): pp. 149–154. DOI 10.2118/950149-G.

[18] Wolfram, J. "On alternative approaches to linearization and Morison's equation for wave forces." *Proceedings of the Royal Society of London. Series A: Mathematical, Physical and Engineering Sciences* Vol. 455 No. 1988 (1999): pp. 2957–2974. DOI 10.1098/rspa.1999.0434.

[19] DNV GL. "DNV-RP-H103: Modelling and Analysis of Marine Operations." Recommended Practice DNV-RP-H103. DNV GL. 2011.

[20] Burton, T. (ed.). *Wind Energy Handbook*, 2nd ed. Wiley (2011).

[21] Jonkman, J. M., Butterfield, S., Musial, W. and Scott, G. "Definition of a 5-MW Reference Wind Turbine for Offshore System Development." Technical Report No. NREL/TP-500-38060. National Renewable Energy Lab. (NREL), Golden, CO (United States). 2009. DOI 10.2172/947422.

[22] Bak, C., Zahle, F., Bitsche, R., Kim, T., Yde, A., Henriksen, L., Andersen, P. B., Natarajan, A. and Hansen, M. H. "Design and performance of a 10 MW wind turbine." *Wind Energy* Vol. 124 (2013).

[23] Tian, X. "Design, Numerical Modelling and Analysis of TLP Floater Supporting the DTU 10MW Wind Turbine." Master's, Norwegian University of Science and Technology. 2016.

[24] SINTEF Ocean. *SIMO User Guide*, Version 4.2.

[25] SINTEF Ocean. *RIFLEX User Guide*, Version 4.2.

[26] Hegseth, J. M., Bachynski, E. E. and Martins, J. R. "Integrated Design Optimization of Spar Floating Wind Turbines." *Marine Structures* Vol. 72 : p. 102771. DOI 10.1016/j.marstruc.2020.102771.

[27] Low, Y. "Frequency domain analysis of a tension leg platform with statistical linearization of the tendon restoring forces." *Marine Structures* Vol. 22 No. 3 (2009): pp. 480–503. DOI 10.1016/j.marstruc.2009.01.002. URL https://doi.org/10.1016/j.marstruc.2009.01.002.

[28] Lee, C.-H. and Newman, J. N. "Computation of wave efects using the panel method." Vol. 1 (2005): p. 211–251. DOI 10.2495/978-1-85312-837-0/06.

[29] Martins, J. R. R. A. and Ning, A. *Engineering Design Optimization*. Cambridge University Press (2022).

[30] Gray, J. S., Hwang, J. T., Martins, J. R. R. A., Moore, K. T. and Naylor, B. A. "OpenMDAO: An Open-Source Framework for Multidisciplinary Design, Analysis, and Optimization." *Structural and Multidisciplinary Optimization* Vol. 59 No. 4 (2019): pp. 1075–1104. DOI 10.1007/s00158-019-02211-z.

[31] Wu, N., Kenway, G., Mader, C. A., Jasa, J. and Martins, J. R. R. A. "pyOptSparse: A Python framework for large-scale constrained nonlinear optimization of sparse systems." *Journal of Open Source Software* Vol. 5 No. 54 (2020): p. 2564. DOI 10.21105/joss.02564.

[32] Hwang, J. T. and Martins, J. R. "A Computational Architecture for Coupling Heterogeneous Numerical Models and Computing Coupled Derivatives." *ACM Trans. Math. Softw.* Vol. 44 No. 4 (2018): pp. 37:1–37:39. DOI 10.1145/3182393.

[33] Gill, P. E., Murray, W. and Saunders, M. A. "SNOPT: An SQP Algorithm for Large-Scale Constrained Optimization." *SIAM Review* Vol. 47 No. 1 (2005): pp. 99–131. DOI 10.1137/S0036144504446096.

[34] Hwang, J. and Martins, J. R. R. A. "GeoMACH: Geometry-Centric MDAO of Aircraft Configurations with High Fidelity." (2012). DOI 10.2514/6.2012-5605.

[35] European Committee for Standardization. "Eurocode 3: Design of Steel Structures, Part 1-6: Strength and Stability of Shell Structures." Technical Report No. EN 1993-1-6: 2007. 2007.

[36] DNV GL. "DNV-OS-J103: Design of Floating Wind Turbine Structures." Offshore Standard DNV-OS-J103. DNV GL. 2013.

[37] DNV GL. "DNV-RP-C203: Fatigue Design of Offshore Steel Structures." Recommended Practice DNV-RP-C203. DNV GL. 2010.

[38] Naess, A., Stansberg, C. T. and Batsevych, O. "Prediction of Extreme Tether Tension for a TLP by the AUR and ACER Methods." *Journal of Offshore Mechanics and Arctic Engineering* Vol. 134 No. 2 (2011). DOI 10.1115/1.4004954. URL https://doi.org/10.1115/1.4004954.

[39] Johannessen, K., Meling, T. S. and Haver, S. "Joint Distribution For Wind And Waves In the Northern North Sea." *International Journal of Offshore and Polar Engineering* Vol. 12 No. 01 (2002).

[40] Chen, C.-T. *Linear System Theory and Design*, fourth edition ed. The Oxford Series in Electrical and Computer Engineering, Oxford University Press (2013).

APPENDIX A. STATESPACE EQUATION OF MOTION

A state-space model is used to represent the linear time-invariant dynamic system that describes the floating wind turbine following work by Hegseth [12]. The state-space approach in TLPOpt combines two models, one for the structural or physical system, and another for the controls system, into a single closed loop linear system. Each state-space model (and the total closed loop system) can be written as a system of equations following the format of Eq. (6). The state vector ($\vec{x}$) and inputs vector ($\vec{u}$) for the closed loop system are given in Eq. (7), for a model with N modes of response considered. To create the closed-loop system, the outputs ($\vec{y}$) from the structural model are set equal to the inputs ($\vec{u}$) of the controls model, and the outputs from the controls model set equal to the controls inputs (not included in Eq. (7)) for the structural model. The closed loop system state-space matrices can then be written as concatenations of the matrices from each model shown in Eq. (8). The closed loop system is used to develop the generic transfer function Eq. (9), for the linearized system based on the formulation from Chen [40]. A more detailed description of these models is given in Hegseth's PhD thesis [12].

$$\begin{aligned} \dot{\vec{x}}(t) &= \mathbf{A}\vec{x}(t) + \mathbf{E}\vec{u}(t) \\ \vec{y}(t) &= \mathbf{C}\vec{x}(t) + \mathbf{D}\vec{u}(t) \end{aligned} \tag{6}$$

$$\begin{aligned} \vec{x} &= \begin{bmatrix} x_1 & \cdots & x_N & \dot{x_1} & \cdots & \dot{x_N} & \dot{\varphi} & \varphi_{lp} & \dot{\varphi}_{lp} \end{bmatrix}^T \\ \vec{u} &= \begin{bmatrix} v_{F_T} & v_{M_T} & v_{Q_A} & e^{i(\omega t)} & \cdots & e^{i(\omega t)} \end{bmatrix}^T \end{aligned} \tag{7}$$

$$\mathbf{A} = \begin{bmatrix} \mathbf{A_s} & \mathbf{E_{sc}}\mathbf{C_c} \\ \mathbf{E_c}\mathbf{C_s} & \mathbf{A_c} \end{bmatrix}, \quad \mathbf{E} = \begin{bmatrix} \mathbf{E_{sd}} \\ \mathbf{0} \end{bmatrix}, \quad \vec{x} = \begin{bmatrix} \vec{x}_s \\ \vec{x}_c \end{bmatrix} \tag{8}$$

$$\mathbf{H}(\omega) = \mathbf{C}\Big(i\omega\mathbf{I} - \mathbf{A}^{-1}\Big)\mathbf{E} + \mathbf{D} \tag{9}$$

The structural model follows from standard frequency-domain dynamic analysis, with the addition of a single degree of freedom rotor speed equation of motion. The model includes two states for each structural mode considered ($x_1, \cdots, x_N, \dot{x}_1, \cdots, \dot{x}_N$), and one state for the rotor speed ($\dot{\varphi}$). The state matrix, $\mathbf{A_s}$ is defined by modal inertia (including hydrodynamic added mass), damping, and stiffness matrices for frequency-domain analysis based on Chen [40]. There are two input matrices, one corresponding to external forcing, $\mathbf{E_{sd}}$, and another corresponding to the control inputs $\mathbf{E_{sc}}$. The output matrix, $\mathbf{C_s}$ is a constant and sparse matrix that 'selects' the outputs (in this case, only the rotor speed) from the states. The feedthrough matrix, $\mathbf{D_s}$ is a constant null matrix.

The controls model is based on the baseline generator torque and blade-pitch controller described above. The model includes two states representing low-pass filtered rotor displacement and speed (φ_{lp}, $\dot{\varphi}_{lp}$). The state matrix ($\mathbf{A_c}$) and input matrix ($\mathbf{B_c}$) are developed to filter the rotor speed using a low-pass frequency (ω_{lp}). Two formulations of the output matrix ($\mathbf{C_c}$) are used depending on if the mean wind speed is above or below rated wind speed, outputting either generator torque or blade pitch angle. The feedthrough matrix $\mathbf{D_c}$ is again a constant null matrix.

APPENDIX B. DESIGN VARIABLE BOUNDS

Table 4 provides the bounds on design variables used in optimization.

TABLE 4: BOUNDS ON DESIGN VARIABLES

Variable	Units	Lower Bound	Upper Bound
D_{tower}	[m]	8.0	18.0
t_{tower}	[mm]	60.0	200.0
D_{column}	[m]	12.0	32.0
t_{column}	[mm]	60.0	200.0
T	[m]	25.0	55.0
$s_{pontoon}$	[m]	4.0	10.0
$t_{pontoon}$	[mm]	44.0	200.0
$L_{pontoon}$	[m]	15.0	45.0
D_{tend}	[m]	0.5	3.0
BF	[-]	1×10^{-6}	1.0